Non-hydrolytic sol–gel synthesis of polypropylene/TiO$_2$ composites by reactive extrusion

Manon Besançon[1] · Yanhui Wang[2] · Noëllie Ylla[1] · Valentin Cinquin[1] · Hubert Mutin[2] · Johan Alauzun[2] ·
Eliane Espuche[1] · Véronique Bounor-Legaré [iD][1]

Abstract

An original way to synthesise polypropylene/titanium dioxide (PP/TiO$_2$) composites combining non-hydrolytic sol–gel chemistry and reactive extrusion was reported. The non-hydrolytic sol–gel reaction between titanium alkoxide as a titanium dioxide precursor and an acid anhydride as an oxygen donor at 240 °C was first evaluated and optimised in an alkane liquid medium. TiO$_2$ was present essentially in crystalline anatase form when synthesised in squalane with a domain size around 10 nm. Based on these encouraging results, the synthesis was adapted to reactive extrusion that means at high temperature in molten viscous polypropylene and for short reaction times (few minutes maximum). The proof of concept was evidenced through the formation of amorphous TiO$_2$-based inorganic domains of size around 1 µm within the polymer matrix from the reaction between titanium isopropoxide and acetic anhydride. A condensation degree of 79% was obtained. To optimise the polymer/filler interface, titanium dioxide precursors and oxygen donors with different alkyl chain lengths were evaluated. Hexanoic anhydride as substituent of acetic anhydride and titanium tetrakis 2-ethylhexyloxide as substituent of titanium isopropoxide were used. The oxygen donor contribution appeared to be dominant for the particle dispersion state. The polypropylene (PP)/TiO$_2$ composite synthesised from the reaction between titanium isopropoxide and hexanoic anhydride showed the narrowest TiO$_2$ particle diameter distribution with a mean particle size around 700 nm.

✉ Véronique Bounor-Legaré
veronique.bounor-legare@univ-lyon1.fr

1   Univ Lyon, Université Lyon1, UMR CNRS 5223, Ingénierie des
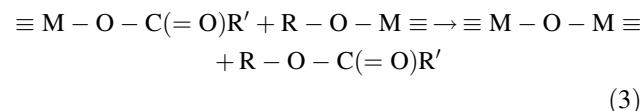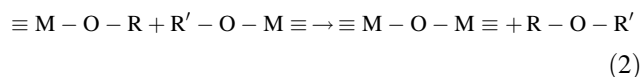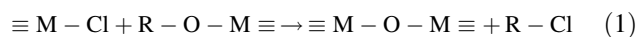   Matériaux Polymères, Lyon, France

2   Institut Charles Gerhardt, Université de Montpellier 2, CNRS
     UMR5253, Montpellier Cedex 5, France

Graphical Abstract

Keywords Non-hydrolytic sol–gel · Reactive extrusion · Titanium dioxide · Polyolefin

Highlights

- Anatase TiO_2 was synthesised at 240 °C in squalane with domain size around 10 nm.
- Amorphous TiO_2 domains were created within the polymer matrix by reactive extrusion.
- Titanium isopropoxide and hexanoic anhydride lead to the narrowest TiO_2 particles.

1 Introduction

Organic/inorganic hybrids and nanocomposites materials have drawn considerable attention due to their potential to enhance structural and functional properties of polymer-based systems. The key parameter for such improvement is the controlled dispersion of inorganic nanofillers. Actually, when well-dispersed, a small amount of inorganic fillers with nanometre size can significantly improve the composite properties, such as mechanical performance [1], flame retardance [2] or gas permeability [3] while maintaining transparency.

The common way to elaborate nanocomposites is the 'top-down' approach, i.e. the dispersion of preformed nanometre-sized fillers into the polymer. These fillers usually consist of elementary nanoparticles forming agglomerates with dimensions up to the micrometre scale. To reach dispersion at the nanometre scale, interactions between particles must be broken by thermomechanical strain. Moreover, modification of the filler and/or the polymer matrix must often be carried out to promote filler/matrix interactions [4, 5]. Despite these approaches, the dispersion of individual nanofillers is usually difficult to

achieve, particularly in the case of hydrophilic nanofillers and hydrophobic polymers such as polyolefins because of their poor compatibility. In addition, another obstacle to the development of nanocomposites is the increasing concerns about nanoparticle manipulation [6]. To overcome these limitations, a 'bottom-up' approach has been developed for the past 20 years, combining reactive extrusion and sol–gel chemistry [7]. Up to now, this approach has been exclusively centred on the hydrolytic sol–gel process. Several works have shown the possibility of generating in situ titanium dioxide nanoparticles in a PP matrix [8, 9]. Kaneko et al. [8] proposed a strategy to synthesise PP/TiO$_2$ nanocomposites based on a catalysed in situ sol–gel reaction during melt mixing. More specifically, PP/TiO$_2$ nanocomposites were obtained by melt mixing PP powder preliminarily impregnated with different titanium alkoxides (titanium n-butoxide, titanium ethoxide or titanium isopropoxide) and a catalytic component (bis(1,2,2,6,6-pentamethyl-4-piperidyl) sebacate or citric acid). The dispersion of the obtained nanoparticles with size below 10 nm required 6 h of impregnation time and the presence of the catalytic component. Another study dedicated to PP/TiO$_2$ synthesis by in situ sol–gel chemistry was conducted by Bahloul et al. [9, 10]. They demonstrated the influence of water incorporated during reactive extrusion on the final nanocomposite morphologies. Titanium n-butoxide was incorporated in the molten PP during extrusion performed at 200 °C. Without water incorporation, the formation of small titanium oxo-organo clusters was favoured, creating an inorganic network consisting of nanometric fillers in the matrix. A post-treatment consisting of the immersion of the obtained PP/TiO$_2$ nanocomposite in water at 80 °C for 72 h allowed a better conversion rate, superior to 95%. The particle diameter obtained after a post-treatment remained below 10 nm. It was shown that the addition of water in the extruder at a high temperature also enhanced the conversion rate of sol–gel reactions and the condensation degree (CD) of TiO$_2$ particles, but favoured nanoparticle agglomeration. The size of these agglomerates was ~200 nm. The surface of such inorganic phase presented hydroxyl groups and consequently had a poor compatibility with the hydrophobic polypropylene matrix.

The non-hydrolytic sol–gel (NHSG) process has been extensively studied during the past 30 years and can overcome some limitations of aqueous processes, including the poor dispersion of particles in an organic medium [11]. The specificities of NHSG chemistry are the use of an organic oxygen donor instead of water and the ability to control the shape and the size of nanoparticles [12]. The NHSG process takes place in non-aqueous media and is based on thermoactivated reactions between a metal or a silicon precursor and an oxygen donor other than water. NHSG routes to oxides have been extensively studied and reviewed [13, 14].

Three main routes can be highlighted: the alkyl halide elimination route involving the condensation between metal alkoxides and metal halides (Eq. (1)), the ether elimination route by a reaction between two metal alkoxides (Eq. (2)) and finally the ester elimination process involving the reaction between metal carboxylates and metal alkoxides (Eq. (3)).

$$\equiv M - Cl + R - O - M \equiv \rightarrow \equiv M - O - M \equiv + R - Cl \quad (1)$$

$$\equiv M - O - R + R' - O - M \equiv \rightarrow \equiv M - O - M \equiv + R - O - R' \quad (2)$$

$$\equiv M - O - C(=O)R' + R - O - M \equiv \rightarrow \equiv M - O - M \equiv + R - O - C(=O)R' \quad (3)$$

One of the most widely explored approaches to synthesise titanium dioxide nanoparticles was the use of metal halides as a precursor via an alkyl halide elimination route. Trentler et al. [15] were the first to describe the synthesis of crystalline anatase nanoparticles based on the reaction of titanium tetrachloride with titanium isopropoxide Ti(O^{i}Pr)$_4$ in trioctylphosphine oxide/heptadecane at 300 °C. The reaction was completed within 5 min and led to the formation of anatase nanoparticles with crystalline domains diameter below 10 nm. Niederberger et al. [16] synthesised anatase nanoparticles from the reaction between titanium tetrachloride and benzyl alcohol at 60 or 100 °C for 8 h followed by an aging for several days. Recently, Wang et al. [17] described the synthesis of mesoporous TiO$_2$ by a reaction between Ti(O^{i}Pr)$_4$ and acetic anhydride (Ac$_2$O) at 200 °C for 12 h. Many publications have described the synthesis of TiO$_2$ nanoparticles in solvent medium, but up to now only a few studies have focused on the in situ synthesis of particles by the NHSG process in a polymer matrix. Morselli et al. [18] synthesised poly(methyl methacrylate)-TiO$_2$ nanocomposite by an in situ NHSG reaction between titanium tetrachloride and benzyl alcohol. The polymer matrix was dissolved in benzyl alcohol at 70 °C and then the titanium dioxide precursor was added at room temperature. After 15 min, the solution was heated at 70 or 100 °C for 24 h. Well-distributed spherical anatase particles of about 30 nm were obtained.

To the best of our knowledge, the use of NHSG in molten polymers during an extrusion process remains unexplored in the literature and could represent an elegant way to synthesise nanocomposites without the manipulation of nanoparticles or solvent. Specific properties such as mechanical barriers, for example, can be envisioned while maintaining transparency. The aim of this article was thus to propose a new route to generate TiO$_2$ nanoparticles in a bottom-up approach combining NHSG reactions and

reactive extrusion. For that goal, the synthesis of TiO_2 particles was first performed at 240 °C for 1 h from titanium isopropoxide and acetic anhydride (Ac_2O) in a model apolar liquid medium in order to evaluate the reactivity. Reactions were then transposed into molten polymer medium to synthesise PP/TiO_2 composites for an expected filler concentration of 5 wt%. Then, in order to improve the dispersion state of synthesised TiO_2 particles in the hydrophobic polymer matrix, another titanium dioxide precursor and an acid anhydride with longer alkyl chains than Ac_2O were investigated. By-products of NHSG reactions were studied and the morphology and linear viscoelastic behaviour of composites in the molten state were investigated in order to evaluate the influence of the different reactants on particle size and dispersion.

2 Experimental part

2.1 Chemicals

The PP («Moplen HP500N») used in this work was provided by LyonDellBasell. The melt flow rate was 12 g in 10 min (230 °C/2.16 kg). Squalane (98%) was purchased from Alfa Aesar. TiO_2 Aeroxide P25 nanoparticles with a primary particle size of about 21 nm were purchased from Sigma Aldrich and used to prepare the PP/TiO_2 nanocomposite reference. The structure of the reactants used to in situ synthesise the TiO_2 nanoparticles were presented in Table 1. Titanium (IV) isopropoxide ($Ti(O^iPr)_4$) 97%, tetrakis 2-ethylhexyl orthotitanate $Ti(2\text{-}OEtHex)_4$ 97% and hexanoic anhydride (Hex_2O_3) 97% were purchased from ABCR. Acetic anhydride (Ac_2O) ≥99% was purchased from Carlo Erba. All chemicals were used without further purification. Some of their properties are depicted in Table 1.

2.2 TiO₂ synthesis in squalane

These syntheses were carried out in a glovebox under argon atmosphere (<10 ppm of water and O_2). $Ti(O^iPr)_4$ (1.57 g,
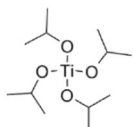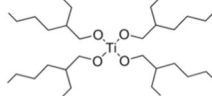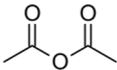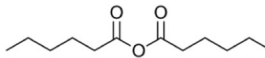
5.5 mmol), Ac_2O (1.12 g, 11.0 mmol) and 10 mL (8.1 g) of squalane were mixed in a stainless steel digestion vessel equipped with a PTFE (polytetrafluoroethylene) lining (23 mL). Then, the sealed autoclave was heated in an oven at 240 °C for 1 h under autogenous pressure. The temperature was chosen according to extrusion process temperature. After this reaction step, the resulting white precipitate was washed with $CHCl_3$ (30 mL, five times) and then acetone (30 mL, five times). The precipitate was dried under vacuum at room temperature and then ground into a fine white powder.

2.3 TiO₂ synthesis in molten PP

A PP/TiO_2 nanocomposite reference with 5 wt% fillers was prepared in a Haake Plasticorder® intensive batch mixer equipped with two Rheomix 600 roller rotors running in a counter rotating way. The rotor speed was set at 50 rpm. Commercial TiO_2 was incorporated in molten PP at 200 °C. This temperature was maintained for 5 min then the temperature was gradually increased from 200 to 240 °C (with a heating rate of 10 °C min⁻¹). Finally, the blend was mixed for 15 min after the introduction of reactants.

All other composite materials were prepared using a co-rotating twin screw extruder (Leistritz ZSE18, $D = 18$ mm, $L/D = 60$). The screw profile was represented in Fig. 1. It was composed of conveying elements (GFA and GFF), two reverse elements (one for the PP melting before reactants incorporation and the other one before the extraction of by-products by vacuum pumping) (GFA-L), kneading (KB) and mixing elements (MB). The screw speed was set at 100 rpm. Temperature of each block can be adjusted independently. Polypropylene was incorporated in the block 0 (B0 in Fig. 1) at 200 °C and with a feed rate $Q = 1$ kg h⁻¹. Depending on the reactants nature and reactivity, two strategies of incorporation were followed (specified in Table 2). First, for the samples $Ti(O^iPr)_4$-Ac_2O, $Ti(OEtHex)_4$-Ac_2O and $Ti(O^iPr)_4$-Hex_2O_3, a pre-mixed strategy was required. In those cases, the titanium dioxide precursor and the oxygen donor were first mixed in a Schlenk tube under

Table 1 Structure and selected properties of titanium dioxide precursors and acid anhydrides

	Titanium isopropoxide $Ti(O^iPr)_4$	Tetrakis 2-ethylhexyloxide orthotitanate $Ti(2\text{-}OEtHex)_4$	Acetic anhydride Ac_2O	Hexanoic anhydride Hex_2O_3
Chemical structure				
Molar mass (g mol⁻¹)	284.22	564.75	102.09	214.30
Boiling point (°C)	232	248	140	250

Fig. 1 Screw profile and localization of injection and by-products extraction points

Table 2 Reaction conditions for the synthesis by reactive extrusion of PP/TiO$_2$ composites from different reactants and expected reaction by-products

Sample	Precursor	O-donor[a]	Pre-mixing strategy	Expected by-product	Expected by-product boiling point (°C)	Temperature of B10 block (°C)
Hydrolytic reference	Ti(O^{i}Pr)$_4$	/	/	/	/	240
Ti(O^{i}Pr)$_4$-Ac$_2$O	Ti(O^{i}Pr)$_4$	Ac$_2$O	Yes	Isopropyl acetate	90	240
Ti(OEtHex)$_4$-Ac$_2$O	Ti(2-OEtHex)$_4$	Ac$_2$O	Yes	2-ethylhexyl acetate	199	240
Ti(O^{i}Pr)$_4$-Hex$_2$O$_3$	Ti(O^{i}Pr)$_4$	Hex$_2$O$_3$	Yes	Isopropyl hexanoate	172	240
Ti(OEtHex)$_4$-Hex$_2$O$_3$	Ti(2-OEtHex)$_4$	Hex$_2$O$_3$	No	2-ethylhexyl hexanoate	265	280

[a]Two equivalents relative to the precursor

argon at room temperature for 1 h. Then, this solution was injected in block 2 (B2 in Fig. 1) of the extruder. For the reaction between Ti(OEtHex)$_4$ and hexanoic anhydride (Table 2), hexanoic anhydride was injected directly into block 2 and Ti(2-OEtHex)$_4$ directly into block 3 using liquid pumps. After introduction of the reactants into the molten PP, the temperature was increased up to 240 °C in block 4. A vacuum pumping system was set up (B10 in Fig. 1) in order to extract the by-products. The sample was collected at the die exit and cooled under air flow. A hydrolytic reference was prepared by injecting only the titanium dioxide precursor Ti(O^{i}Pr)$_4$ into block 2 in order to confirm that titanium dioxide precursor hydrolysis was negligible in comparison with the NHSG reaction in our experimental conditions.

All reaction conditions were summarised in Table 2. Mass quantities of the introduced reactants were calculated to theoretically obtain 5 wt% TiO$_2$ in the final PP-based composite, assuming that the reaction was complete. Boiling points (bp) of expected by-products and temperature of the block B10 were also given in Table 2.

Concerning by-product elimination, two cases were encountered depending on the bp. Either all by-products were removed from the composite thanks to vacuum pump degassing (mainly for by-products presenting the lowest bps), or residual by-products remained in the composite (due to their

high bp). In this last case, in order to quantify the final reaction advancements, the residual by-products were extracted by Soxhlet extraction. In detail, 8 g of nanocomposite sample was grounded into a powder and placed in the Soxhlet device. The solvent used for this purification step was ethyl acetate and the extraction took place at 110 °C for 72 h.

2.4 Characterisation techniques

^{1}H NMR spectroscopy analyses of the reaction medium were performed with samples in solution in deuterated chloroform (CDCl$_3$) using a Bruker Avance III 400-MHz spectrometer.

Thermogravimetric analyses (TGA) of polymer and extruded composites were performed with the TA Q600 of TA Instruments. All the experiments were carried out under a helium atmosphere at a flow rate of 60 mL min^{-1}. Samples were heated from room temperature up to 600 °C with a heating rate of 10 °C min^{-1}.

Reactants and by-products present in the composites were identified by coupling techniques based on thermal desorption analysis (TDA), gas chromatography (GC) and mass spectroscopy (MS). TDA experiments were performed with a Turbo Matrix 350 instrument of Perkin Elmer under an inert helium atmosphere at the flow rate of 1 mL min^{-1}. Nanocomposite samples were heated to 200 °C and the

temperature was maintained for 10 min. The released volatiles were transferred to a gas chromatograph Clarus 680 of Perkin Elmer and a mass spectrometer Clarus SQ 8T of Perkin Elmer. Liquid extracted by-products were analysed by GC-MS coupling, with the same equipment as mentioned before.

X-ray photoelectron (XPS) spectroscopy measurements were carried out using a PHI Quantera SXM spectrometer with a non-monochromatised AlKα source. XPS spectra were collected at a 45° take-off angle between the sample and the analyser. The deconvolution of the spectra was carried out using Multipak (PHI) software. Analyses were operated at energy of 280 eV for survey spectra and 140 eV for high resolution spectra.

The powder X-ray diffraction (XRD) pattern of TiO_2 particles synthesised in solvent medium was collected with a PANalytical X'Pert Pro MPD diffractometer using Cu Kα radiation ($\lambda = 1.54$ Å). Data were collected from 15° to 70° in order to evidence the formation of nanocrystals. The crystalline structure of PP/TiO_2 composites was analysed with the same equipment on composites ground to fine powder. Data were collected from 5° to 50° in order to obtain the whole XRD pattern of PP or from 1° to 6° to provide spectra at low angles.

Raman spectroscopy analyses were also conducted to investigate the amorphous or crystalline nature of TiO_2 particles synthesised in molten PP and in the last case, for determining the type of crystalline structure. Raman spectra were obtained with a Horiba Jobin Yvon LabRAM ARAMIS spectrometer equipped with a CCD detector cooled by a Peltier module. Two lasers were used: 473 and 633 nm.

Scanning electron microscopy (SEM) images of TiO_2 particles synthesised in alkane medium were obtained with a Hitachi S-4800 electron microscope by secondary electron detection mode. The SEM observations of PP/TiO_2 composites were performed on a FEI Quanta 250 FEG microscope with a voltage of 10 kV by backscattered electron analysis in order to obtain a good contrast between the polymer matrix and titanium dioxide particles. Observed sections were prepared by cryo-ultramicrotomy at −110 °C. Particles diameters were determined using Image J software. Transmission electron microscopy (TEM) observations were performed on a Philips CM120 microscope with an accelerated voltage of 120 kV. Ultrathin sections were made at −110 °C using a Leica cryo-ultramicrotome equipped with a diamond knife. The thickness of sections was about 80 nm.

Rheological behaviours of the PP matrix and nanocomposites were analysed in order to investigate the in situ generated particles effect on the linear viscoelastic behaviour of nanocomposites. Measurements were performed in linear dynamic mode of shearing on a rheometer ARES G2 of TA Instruments. Parallel plate geometry with a diameter of 25 mm was used. Analyses were carried out at 200 °C

under a nitrogen atmosphere to prevent thermo-oxidative degradation of the samples. A constant deformation ($\gamma = 5\%$) was chosen in the linear viscoelastic region and experiments were performed in the frequency range $10^{-2} < \omega$ (rad s^{-1}) $< 5.10^2$.

Size exclusion chromatography (SEC) analyses were performed on PP and composites ground to fine powder with a Viscotek-Malvern Instrument equipped with a triple detector consisting of a refractive index detector, a viscosimeter and a light scattering detector, with a right-angle light scattering detector (90°) and a low-angle light scattering detector (7°). The polymer was dissolved in 1,2,4 trichlorobenzene at 150 °C and injected into Waters Styragel HT6E columns at a flow rate of 1 mL min^{-1}. The injection volume was 200 μL.

3 Results and discussion

## 3.1 NHSG synthesis of TiO_2 in a model medium

The first objective of this work was to demonstrate the feasibility of the NHSG reaction in conditions as close as possible to extrusion process ones. To meet the specific conditions of reactive extrusion, NHSG reaction had to be carried out at a higher temperature than the polymer melting point. Furthermore, residence time in an extruder was a few minutes, so selected precursors and oxygen donors should be reactive enough to obtain a high degree of condensation. Although the use of titanium halide was the most explored route in conventional approaches, the use of this precursor was not possible in reactive extrusion because of the possible problem of corrosion of the barrel. Wang et al. [17] found that the reaction between $Ti(O^iPr)_4$ and acetic anhydride in stoichiometric conditions at 200 °C led after 12 h to mesoporous TiO_2 in high yields. Based on this work, titanium alkoxides were selected as titanium dioxide precursors and acid anhydrides as oxygen donors, considering the specificities of reactive extrusion. A temperature of 200 °C was suitable for reaction in molten PP, but 12 h was an extremely long reaction time in comparison with the residence time in an extruder (few minutes). Thus, in this part dedicated to the study of reaction in model medium, the reaction temperature was fixed at 240 °C in order to reduce the reaction time.

The reaction between the titanium isopropoxide and the acetic anhydride led to the formation of TiO_2 by an ester elimination mechanism in two steps, involving a first step of acetoxylation (Eq. (4)) and a second step of condensation (Eq. (5)) [17]. The formed ester was the isopropyl acetate (CH_3COO^iPr).
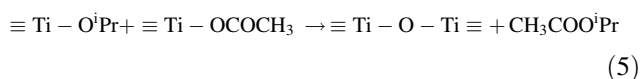
$$\equiv Ti - O^iPr + (CH_3CO)_2O \rightarrow \equiv Ti - OCOCH_3 + CH_3COO^iPr \quad (4)$$
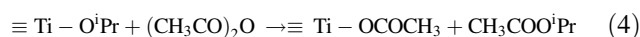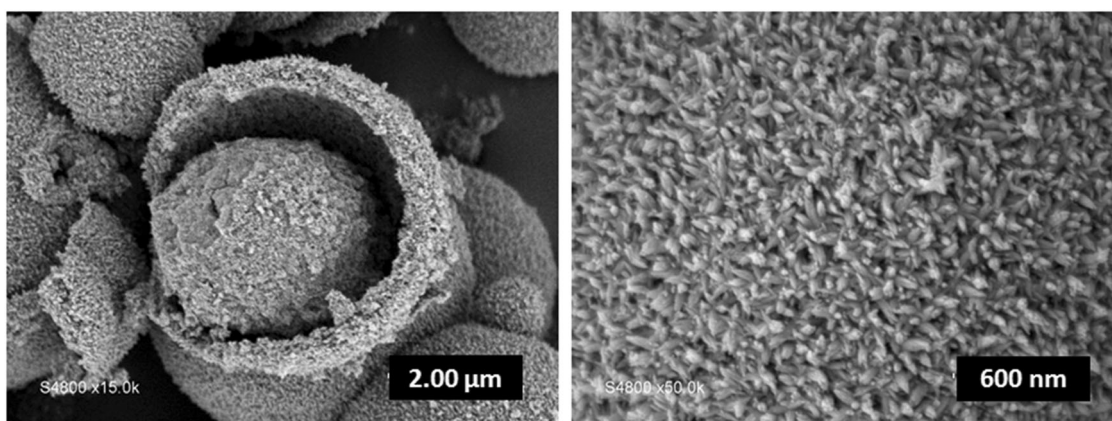
Fig. 2 SEM images of TiO$_2$ particles synthesised from NHSG reaction between Ti(O^{i}Pr)$_4$ and Ac$_2$O in squalane at 240 °C for 1 h
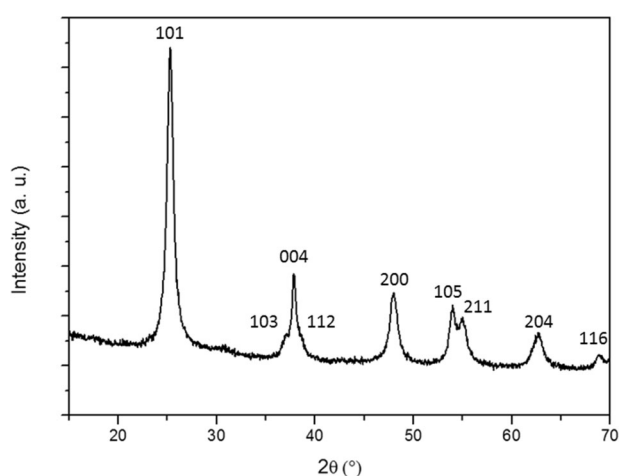
Fig. 3 Powder XRD pattern of TiO$_2$ particles synthesised from NHSG reaction between Ti(O^{i}Pr)$_4$ and Ac$_2$O in squalane at 240 °C for 1 h

$$\equiv Ti - O^iPr + \equiv Ti - OCOCH_3 \rightarrow \equiv Ti - O - Ti \equiv + CH_3COO^iPr \quad (5)$$

In order to evaluate the kinetic of the first reaction step, Ti(O^{i}Pr)$_4$ and Ac$_2$O were mixed without a solvent. According to the ^{1}H NMR analysis of the reaction medium in CDCl$_3$ (Fig. S1 in SI), the acetoxylation reaction was complete after 10 min of mixing at room temperature. Actually, there was no trace of acetic anhydride (characteristic signal at $\delta = 2.22$ ppm), only the presence of isopropyl acetate. Characteristic signals at $\delta = 1.11$ ppm (1), $\delta = 1.89$ ppm (3) and $\delta = 4.86$ ppm (2) were attributed to H atoms of isopropyl acetate in Fig. S1 in SI. The broad signal at around 2 ppm arose from acetate groups linked to TiO$_2$-based domains and broad signal at 1.15 ppm arose from isopropoxide groups linked to TiO$_2$-based domains.

The reaction was carried out at 240 °C for 1 h in squalane, an apolar solvent chosen as the model medium of the

polyolefin. The white precipitate obtained after the reaction in squalane was washed and dried at room temperature. The average yield of recovered product was around 85% regarding the expected amount. The obtained powder was constituted of TiO$_2$ particles with some residual organic groups on the surface.

SEM images of the resulting powder (Fig. 2) showed elongated primary nanoparticles with diameters below 10 nm assembled to form spherical secondary particles of a few micrometres. These results were similar to those of Wang et al. [17] for the TiO$_2$ synthesis in squalane at 200 °C for 12 h.

The XRD pattern of the TiO$_2$ powder was presented in Fig. 3 and showed the presence of diffraction peaks at 25.3°, 37.8° and 47.9° corresponding, respectively, to (101), (004) and (200) crystal planes of anatase form of TiO$_2$ (JCPDS 21-1272) [19]. The intense and narrower (004) reflection compared to the (200) reflection confirmed the presence of anisotropic nanoparticles elongated along the c-axis. The NHSG reaction between Ti(O^{i}Pr)$_4$ and Ac$_2$O provided at 240 °C for 1 h an efficient route to synthesise anatase TiO$_2$ in an apolar solvent.

This study in squalane medium indicated that the non-hydrolytic acetic anhydride route allowed for preparing TiO$_2$ particles in a short time if the reaction temperature was increased to 240 °C. This point was essential for considering the non-hydrolytic synthesis of TiO$_2$ in situ in a molten polymer medium.

3.2 NHSG synthesis of TiO$_2$ in molten PP

3.2.1 Nanocomposites based on Ti(O^{i}Pr)$_4$ and Ac$_2$O as TiO$_2$ precursors

The aim of this part was transposing the NHSG reaction based on Ti(O^{i}Pr)$_4$ and Ac$_2$O performed previously in a liquid alkane medium at 240 °C to a molten polymer

Fig. 4 SEM images of **a** PP/TiO$_2$ nanocomposite reference (5 wt%) and **b** Ti(O^{i}Pr)$_4$-Ac$_2$O composite synthesised by reactive extrusion (5 wt%); TEM images of **c** PP/TiO$_2$ nanocomposite reference (5 wt%), **d** Ti(O^{i}Pr)$_4$-Ac$_2$O composite synthesized by reactive extrusion (5 wt%) and **e** hydrolytic reference from the incorporation of Ti(O^{i}Pr)$_4$ in molten polypropylene
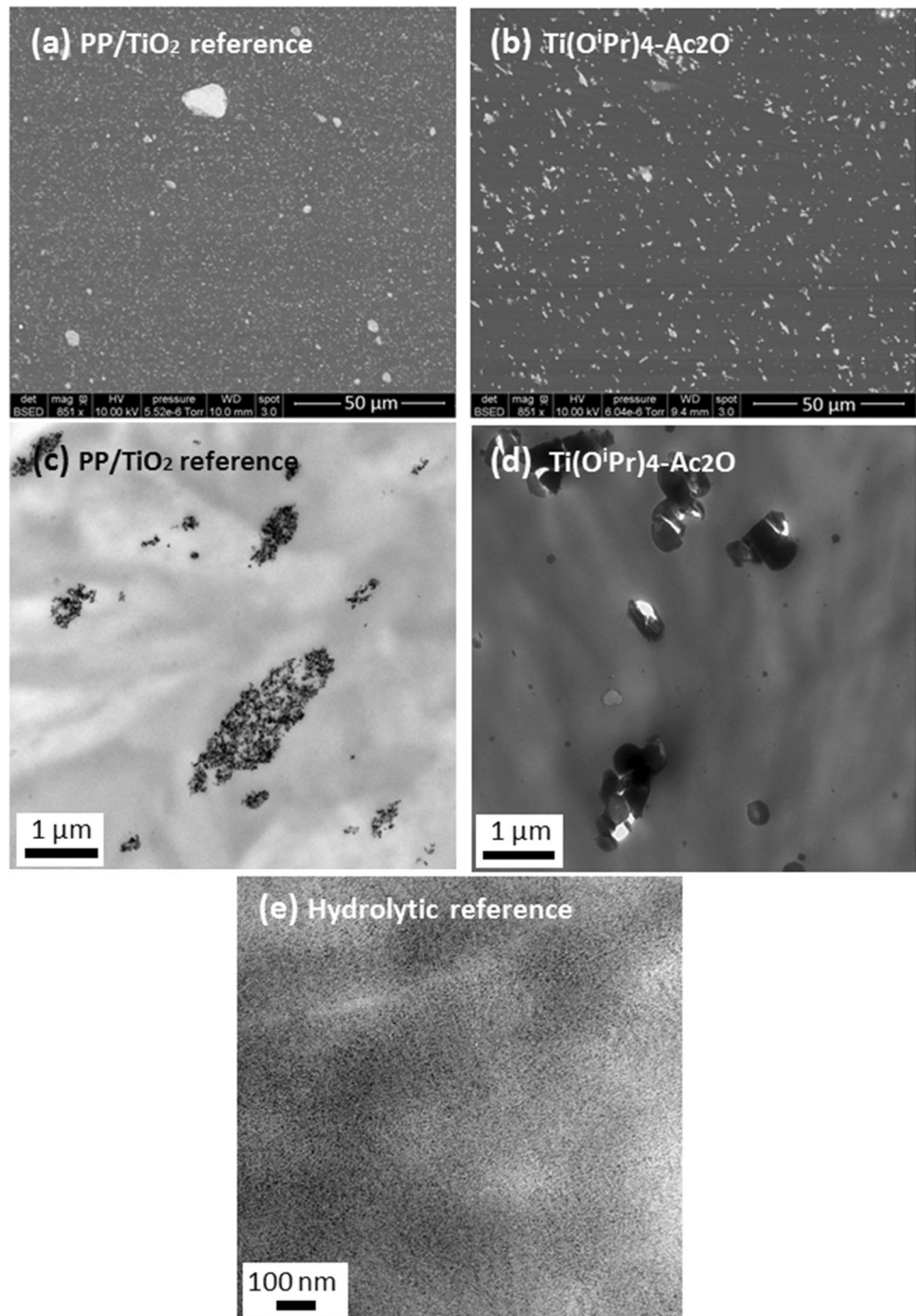
medium in the same range of temperature (the melting point of PP is 160 °C), but for much shorter reaction times (a few minutes instead of 1 h). The experimental conditions were reported in Table 2 line 2 and Fig. 1.

The formation of TiO$_2$-based particles was first demonstrated by electron microscopy analyses and the resulting morphology was compared to that of the PP/TiO$_2$ nanocomposite reference. On the SEM images of the PP/TiO$_2$ nanocomposite reference (Fig. 4a) and the extrudates Ti

(O^{i}Pr)$_4$-Ac$_2$O (Fig. 4b), the TiO$_2$ particles appeared as bright areas. The nanocomposite reference exhibited some particle aggregates of a few micrometres, but the majority of particles were assembled in smaller well-dispersed aggregates, which were also visible on the TEM image of this sample (Fig. 4c). For the Ti(O^{i}Pr)$_4$-Ac$_2$O composite, it appeared that particles were also well-distributed. The mean Feret's diameters of the dispersed particles were determined with the Image J software on the SEM images of the

composites. The mean diameter of aggregates in the PP/TiO$_2$ nanocomposite reference was about 670 nm. For the in situ synthesised Ti(O^{i}Pr)$_4$-Ac$_2$O composite, the mean size was about 1 µm. Finally, the TEM image of Ti(O^{i}Pr)$_4$-Ac$_2$O composite (Fig. 4d) highlighted the presence of smaller particles, below 100 nm in diameter, not included in the mean diameter calculation.

In order to check that formed particles were not the result of the hydrolysis-condensation reactions of Ti(O^{i}Pr)$_4$, TEM micrographs of the hydrolytic reference (Table 2 line 1) (Fig. 4e) were compared with the TEM micrograph of the extrudate Ti(O^{i}Pr)$_4$-Ac$_2$O. No particles were observed at this scale in the hydrolytic reference sample, meaning that hydrolytic sol–gel reaction of Ti(O^{i}Pr)$_4$ was negligible in comparison with NHSG reaction between Ti(O^{i}Pr)$_4$ and Ac$_2$O in the present processing conditions.

As the in situ formation of TiO$_2$-based particles from the NHSG reaction between Ti(O^{i}Pr)$_4$ and Ac$_2$O in the PP matrix was validated, the next step focused on the analysis of the reaction by-products, the extent of the reaction, the CD determined by XPS analysis and finally the particle structure (amorphous or crystalline) elucidated by Raman spectroscopy and XRD analysis.

During the synthesis by reactive extrusion of Ti(O^{i}Pr)$_4$-Ac$_2$O composite, no by-products were recovered thanks to the vacuum pumping system. Moreover TDA-GC-MS coupling analysis (Figure S2 in SI) indicated that there were no remaining by-products in the composite. The only detectable signal on the chromatograph was the water present in the helium flow. No trace of isopropyl acetate was detectable. Actually, as the bp of this expected by-product was 90 °C and thus low compared to reactive extrusion temperature, so it may have evaporated as soon as created.
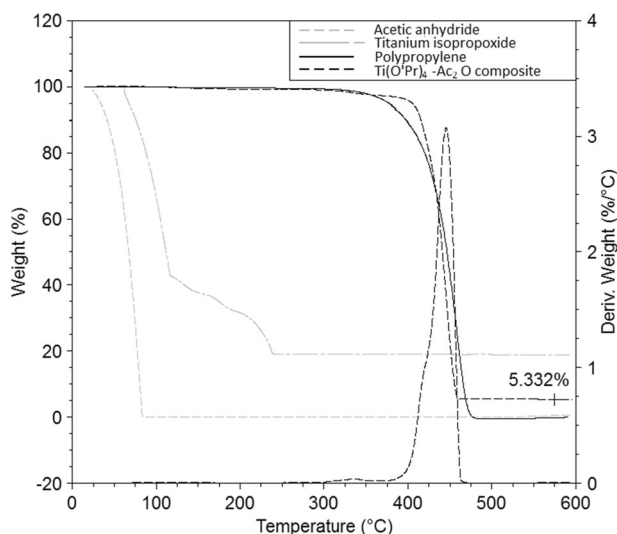
Fig. 5 TGA thermograms obtained under helium atmosphere of extruded polypropylene, Ti(O^{i}Pr)$_4$ and Ac$_2$O reagents and Ti(O^{i}Pr)$_4$-Ac$_2$O composite, heating rate = 10 °C/min

These first analyses were completed by TGA characterisation on the extrudates, which were compared to the thermograms of the pure PP and reagents, respectively. It could have been clearly observed on the thermograms of Fig. 5 that Ac$_2$O had totally evaporated before 250 °C. For Ti(O^{i}Pr)$_4$, 20 wt% of the inorganic residue was observed at a high temperature, corresponding to the expected rate of TiO$_2$ particles formed by calcination. The thermogram of Ti(O^{i}Pr)$_4$-Ac$_2$O composite did not display any mass losses before 300 °C, confirming the absence of residual reactants in the composite. The thermogram also indicated a slight weight loss (1.6 wt%) between 300 and 350 °C, which could have arisen from the creation of isopropyl acetate due to the condensation reactions of residual groups at the surface of TiO$_2$ particles [17]. Polypropylene degradation typically occurs between 310 and 450 °C [20, 21]. TGA of extruded PP and the Ti(O^{i}Pr)$_4$-Ac$_2$O composite showed that PP degradation took place in the same temperature range. The degradation started at a higher temperature for the composite than for the neat PP. The presence of metal could have influenced the degradation behaviour of the polymer. For example, the temperature of PP thermal degradation was lower with the presence of copper than for the neat polymer [22]. However, in numerous studies, the presence of TiO$_2$ particles allowed for improving the thermal stability of PP [23, 24]. Finally, the residue value measured at high temperature (above 500 °C) indicated the amount of inorganic species, equal to 5.3 wt%, which was in good agreement with the theoretical expected one of 5 wt%.

The atomic concentrations of the individual elements were determined by XPS measurements for PP and Ti(O^{i}Pr)$_4$-Ac$_2$O composite (Table 3). Based on the morphological observation, we postulated a homogeneous repartition of the inorganic domains in the PP matrix and thus we considered the overall composition similar to the surface composition.

In the PP reference, the only element found was carbon. Its peak was detected at 285 eV and corresponds to aliphatic carbon C(1s) [25]. In the case of the in situ PP/TiO$_2$ composite, C, O and Ti were detected, as expected. The ratio between Ti and O was different from the expected ratio of a TiO$_2$ contribution. Indeed, for a titanium contribution of 0.2%, the expected oxygen concentration would have been 0.4%, which was significantly different from the effective oxygen concentration that was measured: 0.7%. Three reasons could have explained this difference: the

Table 3 Atomic composition % according to XPS analysis for polypropylene and in situ synthesised Ti(O^{i}Pr)$_4$-Ac$_2$O composite

	C	O	Ti
PP	100	–	–
PP/TiO$_2$ (Ti(O^{i}Pr)$_4$-Ac$_2$O)	99.1	0.7	0.2

measurement uncertainty, the presence of pollution on the composite surface and, as expected, the presence of organic groups on the surface of the particles due to incomplete condensation. In a publication by Bahloul et al. [26], a PP/anatase TiO_2 composite with 9 wt% fillers was analysed by XPS and the chemical composition ratio of the sample (99.6% C; 0.3% O; 0.1% Ti) was approximately the same as the results obtained here.

XPS analysis also provided information about the CD of synthesised titanium dioxide by quantifying Ti–O–Ti bonds in relation to Ti–O–C or Ti–O–H bonds. A detailed analysis of the O(1s) spectrum of the PP/TiO_2 composite (Fig. 6) allowed us to determine the different environments of oxygen atoms in the created nanoparticles. The deconvolution of the O(1s) peak showed that two contributions could be distinguished. The first peak at 529.9 eV was assigned to Ti–O–Ti and the second peak at 531.8 eV to Ti–O–H or Ti–O–C [26–31]. The CD was determined by the respective area of these peaks. The proportion of Ti–O–Ti bonds was associated with the CD. Indeed, 65% of oxygen atoms were involved in Ti–O–Ti bonds and 35% in Ti–O–C or Ti–O–H bonds, which corresponded to the formula $Ti(O)_{1.58}(OR)_{0.84}$. The CD was therefore estimated at 79%. The method used to determine the CD was detailed hereafter.

If we consider that TiO_2 was the formula for a complete condensation (100%) and that $Ti(OR)_4$ was the formula for a non-condensed titanium atom (CD equal to 0%), a CD of 50% corresponded to the formula $Ti(O)_{2-x}(OR)_{2x}$. Consequently, the determined percent of O atoms included in Ti–O–Ti environment by XPS analysis was equal to $(2-x)/((2-x)+2x)$. The CD was then obtained by the following equation: $CD = 100*(2-x)/2$.

Finally, the $Ti(2p_{3/2})$ binding energy peak was observed at 458.4 eV, corresponding to an oxide form. According to Barlier et al. [28], this value of binding energy corresponded to Ti in an octahedral environment, and therefore to condensed titanium alkoxides. This meant that Ti–O–Ti bond formation resulted in the saturation of the Ti ion coordination sites.

All these data confirmed the in situ creation of TiO_2-based inorganic domains with a high CD by the NHSG reaction in molten PP at a high temperature in a few minutes.

In order to determine if the synthesised particles were crystalline or amorphous, samples were analysed by Raman spectroscopy and XRD. Raman active modes of anatase and rutile TiO_2 were given in Table 4. Compared to neat PP, the Raman spectrum of the PP/TiO_2 reference composite exhibited three additional peaks: a strong peak at 140 cm^{-1} and two weaker ones at 192 and 635 cm^{-1} (Fig. S3 in SI). Based on the data given in Table 4, the presence of these three bands and their respective intensity allowed for identifying the anatase form.
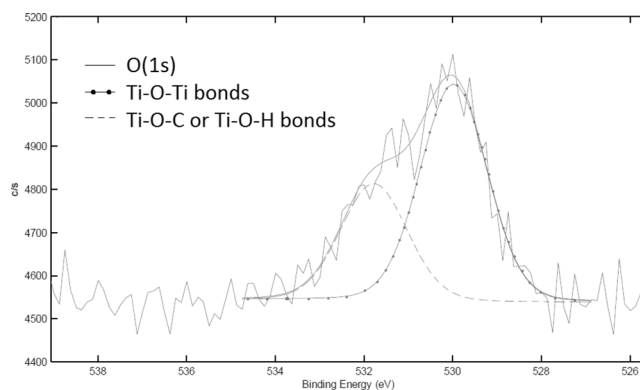

Fig. 6 Deconvolution of the XPS O(1s) peak of the in situ $Ti(O^iPr)_4$-Ac_2O composite

**Table 4** Raman bands of anatase and rutile TiO_2 [45, 46][a]

Anatase band (cm^{-1})	Rutile bands (cm^{-1})
144 (E$_g$) (very strong)	143 (B$_{1g}$) (weak)
197 (E$_g$) (very weak)	235 (B$_{2g}$) (strong)
400 (B$_{1g}$) (very weak)	447 (E$_g$) (very strong)
515 (B$_{1g}$, A$_{1g}$) (very weak)	612 (A$_{1g}$) (very strong)
640 (E$_g$) (weak)	

[a]A and B for singly degenerate wave functions, E for doubly degenerate wave functions, g if the wave function is even
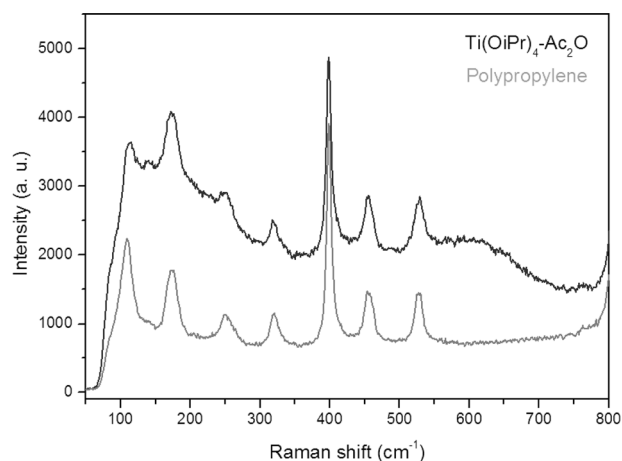
Fig. 7 Raman spectra of the polypropylene and the $Ti(O^iPr)_4$-Ac_2O composite

The Raman spectrum of $Ti(O^iPr)_4$-Ac_2O composite (Fig. 7) exhibited a broad signal at around 600 cm^{-1}, which was not present on the PP spectrum. This signal was not well-defined and therefore did not correspond to a crystalline phase. Huang et al. [32] showed that amorphous TiO_2 exhibits three weak and broad signals at 171, 422 and 616 cm^{-1}. The signal that we observed at around 600 cm^{-1} could therefore correspond to amorphous TiO_2 domains in the composite.
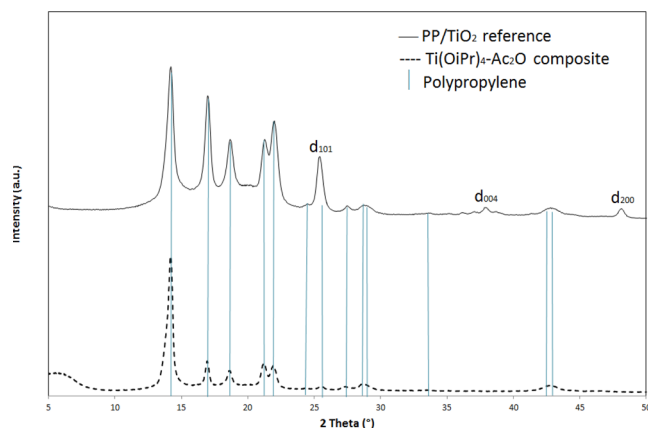
Fig. 8 XRD pattern of Ti(O^{i}Pr)$_4$-Ac$_2$O composite. Comparison with the pattern obtained for the PP/TiO$_2$ composite reference

To complete this analysis, the XRD patterns of PP/TiO$_2$ reference composite and Ti(O^{i}Pr)$_4$-Ac$_2$O composite were shown in Fig. 8. All observed peaks pointed by vertical lines were associated to the crystalline structures of the polymer matrix. According to Karacan and Benli [33], diffraction peaks at 14.2°, 16.9° and 18.6° corresponded, respectively, to (110), (040) and (130) crystal planes of the α-monoclinic form of the isotactic PP.

No peaks attributed to the anatase ($2\theta = 25.3°$ for d_{101}, $2\theta = 37.8°$ for d_{004} and $2\theta = 47.9°$ for d_{200}) or rutile ($2\theta = 27.4°$ for d_{110}, $2\theta = 35.9°$ for d_{101} and $2\theta = 39.2°$ for d_{200}) phases of TiO$_2$ were present in the XRD pattern of the Ti (O^{i}Pr)$_4$-Ac$_2$O composite [34], whereas in the PP/TiO$_2$ reference pattern, three peaks associated to anatase structure were present, as expected. None of the typical diffraction peaks associated with TiO$_2$ anatase or rutile forms as previously discussed were observed either by Hu and Marand [35] in the XRD pattern of a poly(amide-imide)(PAI)/TiO$_2$ composite. They synthesised the composite by an in situ hydrolytic sol–gel process from tetraethyl titanate in a dissolved solution of PAI matrix in *N,N*-dimethyl acetamide at room temperature for 36 h. Then the sample was cured at different temperatures (room temperature, 150 and 220 °C) for 76 h. Nanosized TiO$_2$ domains were well-dispersed within the PAI matrix thanks to the hydrogen bonding interactions between the amide groups of the PAI and the hydroxyl groups on the inorganic oxide. The authors explained the absence of diffraction TiO$_2$ peaks by the incomplete condensation, given the presence of unreacted alkoxide and hydroxyl groups. In the present case, the observed size of TiO$_2$ domains, the absence of unreacted reactants and the CD were not in line with this explanation. The absence of diffraction peaks of TiO$_2$ was rather explained by the short reaction time and process conditions when the synthesis was carried out by reactive extrusion. However, in the present XRD pattern, the presence of a

peak at low value of 2θ ($2\theta = 5.4°$) could be observed, not attributed to the PP matrix. Bahloul et al. [26] observed a similar peak in the XRD pattern of PP/TiO$_2$ nanocomposite synthesised by hydrolytic sol–gel process. Their hypothesis was that this peak was a signature of particle organisation at long distances. Wu [36] also identified an additional peak in the XRD patterns of polycaprolactone (PCL)/TiO$_2$ and PCL-graft-acrylic acid/TiO$_2$ nanocomposites at, respectively, $2\theta = 2.9°$ and $2\theta = 2.6°$. He suggested that these low 2θ values were related to greater spacing between TiO$_2$ nanoparticles and implied better filler/matrix interaction.

To conclude this part, contrary to the anatase TiO$_2$ synthesised in squalane, TiO$_2$-based particles synthesised in molten PP were mostly in amorphous form, as can be observed by XRD and Raman analyses. However, the in situ formation of rather well-condensed TiO$_2$-based particles by NHSG synthesis in molten PP through the ester elimination reaction between Ti(O^{i}Pr)$_4$ and Ac$_2$O was evidenced. In order to further investigate the potential of such a synthesis, we focused in the second part of this study on the role of the nature of reactants on the reaction kinetics and the final dispersion of the in situ formed particles. In that frame, reactants with longer alkyl chains were used and compared to the first system, e.g. the Ti(O^{i}Pr)$_4$-Ac$_2$O composite.

3.3 Influence of reactants with longer alkyl chains on TiO$_2$ nanoparticle formation and composite morphology

The analysis of the Ti(O^{i}Pr)$_4$-Ac$_2$O composite by electron microscopy allowed us to think that weak interfacial interactions took place between the synthesised fillers and the PP matrix in this system. Actually, in Fig. 4, some particles were ripped out of the polymer matrix during section preparation by cryo-ultramicrotomy. Thus, in order to enhance the interface between the TiO$_2$ particles and the PP matrix, reactants with longer alkyl chains were chosen with the aim of increasing their affinity with the non-polar reaction medium. Tetrakis 2-ethylhexyl orthotitanate was used as a substituent of titanium isopropoxide and hexanoic anhydride as a substituent of acetic anhydride.

Two aspects were considered for the improvement of TiO$_2$-based particles dispersion by the use of these reactants: the first one was the affinity between the PP matrix and the reactants, and the second one was the compatibility between particles once synthesised and PP. In light of the reaction equations (Eqs. (4) and (5)), the surface of TiO$_2$ particles was surrounded by alkoxy groups coming from the oxygen donor and therefore acid anhydrides should have played a predominant role in the dispersion of the in situ formed particles.

Indications about the affinity between the PP and the different reactants were approached thanks to the solubility

parameter δ, which was estimated using Fedors' method [37], even if the temperature and viscosity parameters could not be taken into account in this calculation. In the literature, δ values of PP are between 15.8 and 18.8 $(MPa)^{1/2}$ [38, 39], close to the calculated value of 16.0 $(MPa)^{1/2}$. The calculated solubility parameter of each reactant was reported in Table 5. As the solubility parameter δ values of the titanium dioxide precursors $Ti(O^iPr)_4$ and $Ti(2-OEtHex)_4$ were very close to each other, i.e. 16.5 and 16.8 $(MPa)^{1/2}$, respectively, no impact of their solubility in the PP matrix was observed, despite of the difference in alkyl chain length. However, analysing the solubility parameters of oxygen donors, the use of hexanoic anhydride should have favoured the miscibility with PP. Indeed, its solubility parameter δ of 18.3 $(MPa)^{1/2}$ was closer to the PP solubility parameter than to the solubility parameter δ of acetic anhydride. So, hexanoic anhydride should have been better dispersed in the polyolefin molten polymer and should have provided a better dispersion of particles thanks to the hexyl groups at the surface of TiO_2 particles created in situ.
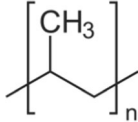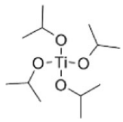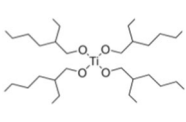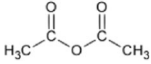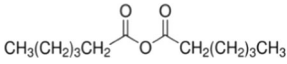
These different reactants were used for the NHSG synthesis of PP/TiO_2 composites in order to evaluate their impact on the composite morphology. Reactions were summarised in the experimental part, Table 2. For all the synthesised (Ti $(O^iPr)_4$-Hex_2O_3, $Ti(OEtHex)_4$-Ac_2O and $Ti(OEtHex)_4$-Hex_2O_3) composites, but not for the $Ti(O^iPr)_4$-Ac_2O composite, some of the by-products could have been extracted by vacuum pumping. These by-products were characterised by GC-MS coupling analysis (Fig. S4 in SI). In all three cases, the expected by-product was detected. For the $Ti(OEtHex)_4$-Ac_2O, $Ti(O^iPr)_4$-Hex_2O_3 and $Ti(OEtHex)_4$-Hex_2O_3 composites, corresponding esters (2-ethylhexyl acetate, isopropyl hexanoate and 2-ethylhexyl hexanoate) had elution times of 5.5, 4.5 and 7.7 min, respectively. The presence of alcohol detected in different composites (2-ethylhexanol with an elution time between 4 and 5 min for the $Ti(OEtHex)_4$-Ac_2O and $Ti(OEtHex)_4$-Hex_2O_3 composites; propan-2-ol with an elution time at 1.9 min for the $Ti(O^iPr)_4$-Hex_2O_3 composite) could have suggested a contribution from hydrolytic reactions, but a low proportion of the corresponding alcohol was already present in the commercial precursors. It was noteworthy that no acid anhydride was detected, confirming that the acetoxylation step was complete before the extraction zone. For the $Ti(O^iPr)_4$-Hex_2O_3 and $Ti(OEtHex)_4$-Ac_2O samples, the bps of the esters were lower than the extrusion temperature and a part of them had evaporated at the die exit, which hindered a complete quantitative evaluation of the by-product. On the contrary, for the last sample ($Ti(OEtHex)_4$-Hex_2O_3), the ester by-product presented a higher bp than the reactive extrusion temperature and remained in the composite and may have modified the nature of the matrix (no pure PP) and thus the expected compatibilisation based on the calculation of solubility parameters.

From the Soxhlet extraction, the remaining by-product in the $Ti(OEtHex)_4$-Ac_2O, $Ti(O^iPr)_4$-Hex_2O_3 and $Ti(OEtHex)_4$-Hex_2O_3 composites corresponded to 3.11, 2.15 and 17.0 wt%, respectively, of the initial composite mass. For $Ti(OEtHex)_4$-Ac_2O and $Ti(O^iPr)_4$-Hex_2O_3, as described previously, a part of by-products had evaporated during the extrusion process. However, for the last composite $Ti(OEtHex)_4$-Hex_2O_3, the mass balance of the reaction could be established from the quantity of by-products extracted by vacuum pumping and by Soxhlet extraction. Experimentally, 35 wt% of by-products were extracted from the composite, very close to the theoretical value of 36 wt% expected for a total condensation reaction. The ^1H NMR spectrum of the extracted medium (Fig. S5 in SI) showed the presence of the expected ester by the chemical shifts at 2.2 and 3.9 ppm and 2-ethyl-1-hexanol by the chemical shift at 3.5 ppm (corresponding to a contribution of 7% of the hydrolytic reaction of the titanium dioxide precursor). A conversion rate close to 93% was determined from this method. However, it should be noted that condensation reactions may continue throughout the Soxhlet extraction at 110 °C, although shorter extraction times (24 or 48 h) led to the same CD. It was noteworthy that there was no signal for hexanoic anhydride, again demonstrating that the first step of the reaction, e.g. acetoxylation, was complete.

Extruded composites were characterised by SEM and TEM to compare the particle dispersion states (Fig. 9). By taking as a reference the $Ti(O^iPr)_4$-Ac_2O composite morphology previously analysed, the use of $Ti(2-OEtHex)_4$ with acetic anhydride ($Ti(OEtHex)_4$-Ac_2O) did not lead to smaller particles or aggregates, but a finer particle dispersion was observed. This result agreed with the determination of solubility parameters of the two different titanium dioxide precursors. In the TEM micrograph of the $Ti(O^iPr)$

Table 5 Solubility parameter of polypropylene and reactants, calculated through Fedors' method [37]

Product					
	Polypropylene	$Ti(O^iPr)_4$	$Ti(2-OEtHex)_4$	Ac_2O	Hex_2O_3
δ $(MPa)^{1/2}$	16.0	16.5	16.8	19.8	18.3

Fig. 9 SEM images, diameter distribution of particles/ aggregates calculated from SEM images and TEM images of PP/ TiO_2 composites synthesised in situ by reactive extrusion
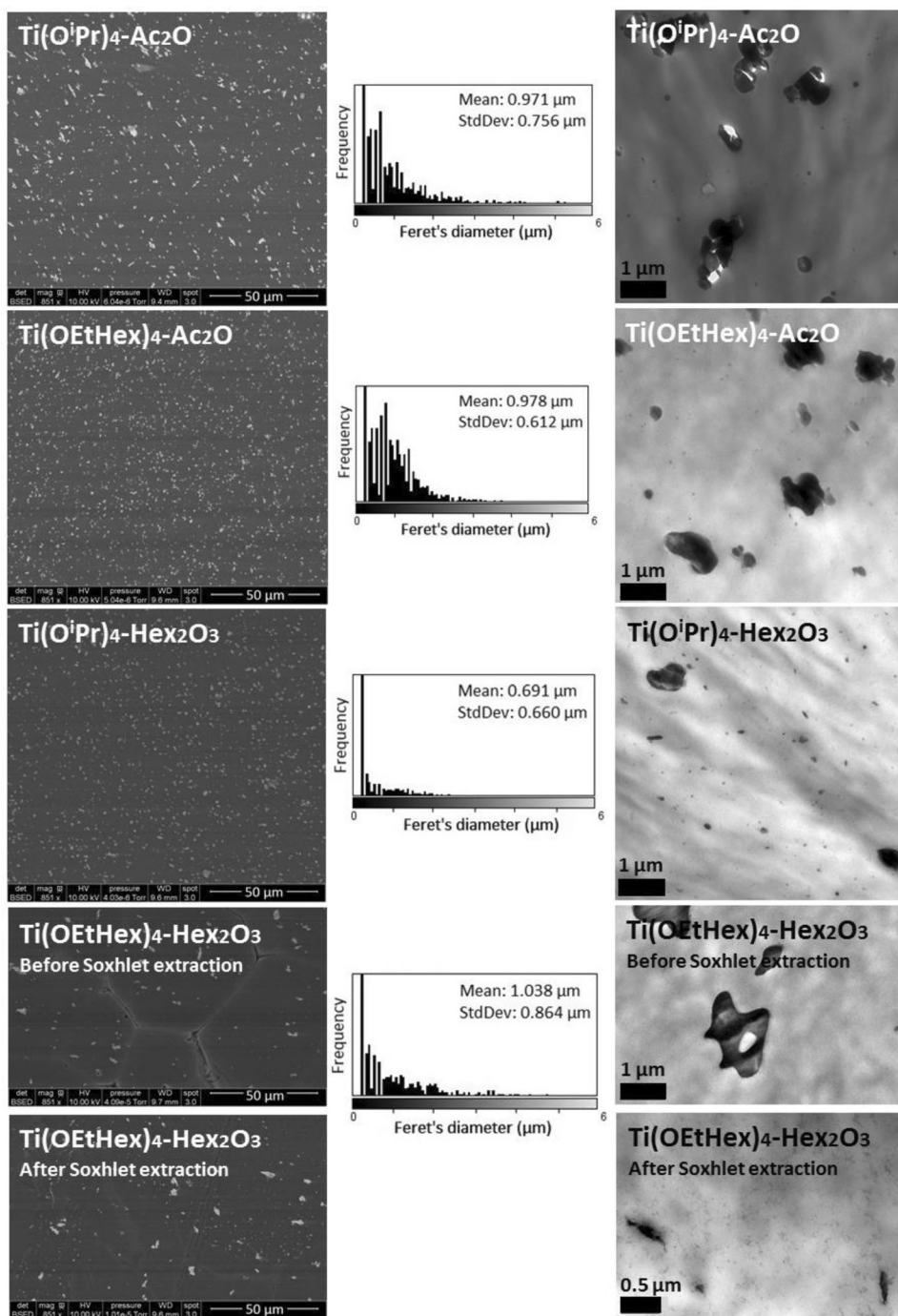
$_4$-Ac_2O sample, some holes were observed at the interface between the polymer matrix and agglomerates. However, particles of the Ti(OEtHex)$_4$-Ac_2O composite were not ripped from the PP matrix during sample preparation, which evidenced a better interface with PP. Besides, SEM and TEM images of the sample Ti(O^{i}Pr)$_4$-Hex_2O_3 displayed the finest particle dispersion, revealing as predicted previously a better dispersion of the reactant in the PP matrix and a better dispersion of the in situ created TiO_2 particles, due to the presence of hexyl chains at the surface of particles.

Based on these assessments, good dispersion and small particle diameter may have been expected for the sample Ti (OEtHex)$_4$-Hex_2O_3, given the long alkyl chains of reactants. Nevertheless, from SEM observations, it was found that particle/aggregate diameters were the largest of the four samples. A possible explanation for such a result was the high quantity of the remaining by-products that may have formed non-miscible domains (where TiO_2-based particles could preferentially grow). Thus, the presence of these separated phases within the polymer matrix could have

favoured the agglomeration of the created TiO$_2$ particles through higher affinities towards this phase in comparison to the PP matrix. It was noteworthy that in the transmission electron micrograph of the sample after by-product extraction, it was observed, in addition to the previously discussed micrometric TiO$_2$ domains, nanoparticles with a diameter <10 nm (micrograph at bottom right in Fig. 9). These nanoparticles formed a network that was visible only after by-product extraction and only in the Ti(OEtHex)$_4$-Hex$_2$O$_3$ sample, showing the effect of alkyl chain length on the in situ formation of TiO$_2$-based particles.

XRD analyses carried out on these samples showed the absence of anatase and rutile peaks, as for the Ti(O^{i}Pr)$_4$-Ac$_2$O sample. The peak observed at 5.4° in the XRD pattern of Ti(O^{i}Pr)$_4$-Ac$_2$O seemed to be shifted towards small angles for the new studied samples (Fig. 10). Indeed, for Ti(OEtHex)$_4$-Ac$_2$O composite, the signal was centred at around 4.3° and for both Ti(O^{i}Pr)$_4$-Hex$_2$O$_3$ and Ti(OEtHex)$_4$-Hex$_2$O$_3$ composites, the signal was centred at 3.9°. As discussed before, this corresponded to an improvement in TiO$_2$-based particle dispersion, as seen by Wu et al. [36]. Moreover, the peak intensity was greatest for the Ti(O^{i}Pr)$_4$-Hex$_2$O$_3$ composite, which may have been correlated with a homogeneous distribution of TiO$_2$-based particles in the PP matrix.

Finally, the viscoelastic behaviour of PP/TiO$_2$ composites in the melt state was investigated to provide complementary information on filler/matrix interactions. According to the Einstein law (Eq. (6)) that predicted the impact of the addition of particles on the viscoelastic behaviour of a material, the introduction of 5 wt% of

microparticles should not affect the viscoelastic behaviour of the PP matrix (Fig. 11).

$$G^*(\omega) = G_m^*(\omega) \left(\frac{1 + \frac{3}{2}\varphi_r}{1 - \varphi_r} \right) \qquad (6)$$

where G^* and G_m^* were, respectively, the complex shear modulus of the composite and of the PP matrix, and ϕ_r was the volume fraction of TiO$_2$ particles, $\phi_r = 0.012$ in this case.

Nevertheless, the in situ synthesis of nanoparticles did not lead necessarily to the same viscoelastic behaviour, as demonstrated by Bahloul et al. [40]. For a TiO$_2$ particle concentration of 6 wt%, the authors observed the appearance of a plateau at low frequencies, corresponding to a solid-like behaviour, common for nanocomposite materials. Two mechanisms explained this phenomenon: filler/filler or polymer matrix/filler interactions [41, 42].

In Fig. 11, a modification of the viscoelastic behaviour of in situ PP/TiO$_2$ composites compared with the PP matrix was observed. More precisely, the storage modulus G′ increased at low frequencies, modifying the terminal zone of relaxation. There was no permanent plateau at low frequencies, as generally observed for nanocomposites, but a second relaxation mechanism. The same modification of the storage modulus was reported by Acierno et al. [43] who elaborated PP/TiO$_2$ nanocomposites by introducing TiO$_2$ nanoparticles in the molten PP. The authors related this behaviour to the existence of inorganic nanoparticle clusters, which formed a dynamic population with different kinetics of relaxation to the host polymer. Lacoste et al. [44] also observed a shoulder for G′ at low frequencies when they functionalised PET with new chain extenders. The PET branched structure led to the storage modulus increase. However, in our case, the results of SEC analyses in Table 6 showed that the average molar masses between neat PP and composites remained unchanged. Consequently, the observed modification of viscoelastic behaviour was due to the presence of fillers, as explained by Acierno et al. [43]. It was noteworthy that the increase in the storage modulus was greatest for the composite Ti(OEtHex)$_4$-Hex$_2$O$_3$. The network formed by the very small particles observed in this composite after Soxhlet extraction explained this storage modulus difference due to an increase in particle–particle interactions and the formation of particle aggregates at the nanoscale with a particle size below 10 nm. Indeed, the other composites did not exhibit such small particles.
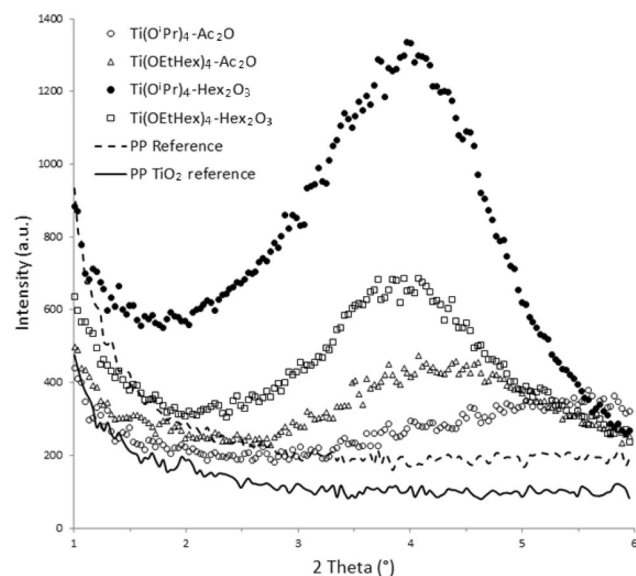
Fig. 10 XRD patterns diffractograms at low angle of polypropylene, PP/TiO$_2$ reference composite and PP/TiO$_2$ composites synthesised by reactive extrusion by NHSG reaction

4 Conclusions

PP/TiO$_2$ composites were originally synthesised by combining a NHSG process and reactive extrusion. First,
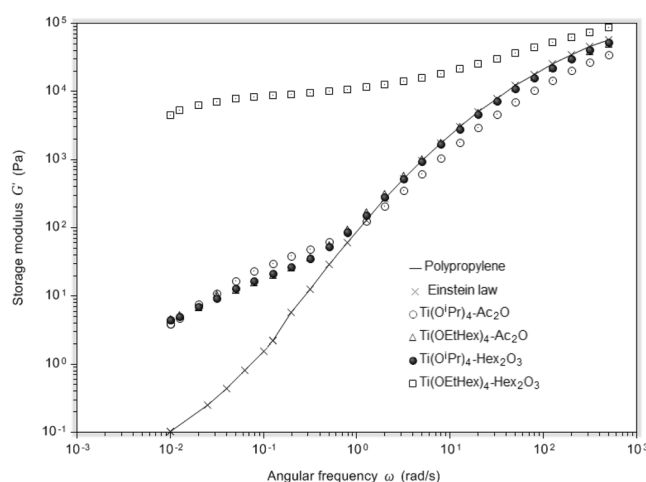
Fig. 11 Viscoelastic behaviour of PP/TiO$_2$ composites after by-products extraction synthesised from NHSG reactions in extruder. Variation of the storage modulus versus frequencies measured under nitrogen atmosphere at 200 °C

Table 6 Size exclusion chromatography results for PP reference and PP/TiO$_2$ composites

	Mn (g mol^{-1})	Mw (g mol^{-1})	Mw/Mn
PP reference	85800	183000	2.13
Ti(O^{i}Pr)$_4$-A$_2$O	84600	181000	2.14
Ti(OEtHex)$_4$-Hex$_2$O$_3$	88300	183000	2.07

syntheses in an alkane medium allowed for determining the reactivity between acetic anhydride and titanium isopropoxide at 240 °C for 1 h, then TiO$_2$-based particles were prepared in situ from this non-hydrolytic reaction in a molten PP matrix. The reaction in model medium led to the formation of anatase particles. Nanorods (about 10 nm) were assembled to form spherical secondary particles of a few micrometres. In PP medium, XPS analysis evidenced the formation of TiO$_2$-based particles by the presence of Ti–O–Ti bonds and allowed for determining a CD of 79%. The mean size of TiO$_2$ particles synthesised in situ in PP was 1 µm. Particles synthesised in situ in molten PP were mostly amorphous, according to Raman spectroscopy and XRD analysis.

To improve the TiO$_2$-based particle dispersion, reactants with longer alkyl chains were used. The finest particle dispersion was obtained with the use of hexanoic anhydride instead of acetic anhydride, with a mean particle size of about 700 nm. This enhancement was partially attributable to hexyl groups remaining at the surface of TiO$_2$-based particles. Rheology measurements showed a modification of the viscoelastic behaviour at low frequencies, indicating the presence of aggregates and filler/matrix interactions. This modification of the storage modulus was greatest for the composite Ti(OEtHex)$_4$-Hex$_2$O$_3$, due to the presence of a network of very small particles in the PP matrix.

Compliance with ethical standards

References

1. Yang J, Zhao J-J, Han C-R, Duan J-F (2014) Keys to enhancing mechanical properties of silica nanoparticle composites hydrogels: the role of network structure and interfacial interactions. Compos Sci Technol 95:1–7. https://doi.org/10.1016/j.compscitech.2014.02.003
2. Laachachi A, Cochez M, Leroy E, Gaudon P, Ferriol M, Cuesta JML (2006) Effect of Al2O3 and TiO2 nanoparticles and APP on thermal stability and flame retardance of PMMA. Polym Adv Technol 17:327–334. https://doi.org/10.1002/pat.690
3. Mangadlao JD, Xu H, Baer E, Advincula RC (2017) In situ photogeneration of palladium nanoparticles in thermoplastic polyurethane: photopatterning and enhanced oxygen barrier property. Macromol Chem Phys 218:1700289. https://doi.org/10.1002/macp.201700289
4. Fages E, Pascual J, Gimeno O, Garcia-Sanoguera D, Balart R (2011) Study of antibacterial properties of polypropylene filled with surfactant-coated silver nanoparticles. Polym Eng Sci 51:804–811. https://doi.org/10.1002/pen.21889
5. Iijima M, Kobayakawa M, Yamazaki M, Ohta Y, Kamiya H (2009) Anionic surfactant with hydrophobic and hydrophilic chains for nanoparticle dispersion and shape memory polymer nanocomposites. J Am Chem Soc 131:16342–16343. https://doi.org/10.1021/ja906655r
6. Radad K, Al-Shraim M, Moldzio R, Rausch W-D (2012) Recent advances in benefits and hazards of engineered nanoparticles. Environ Toxicol Pharmacol 34:661–672. https://doi.org/10.1016/j.etap.2012.07.011
7. Bounor-Legaré V, Cassagnau P (2014) In situ synthesis of organic–inorganic hybrids or nanocomposites from sol–gel chemistry in molten polymers. Prog Polym Sci 39:1473–1497. https://doi.org/10.1016/j.progpolymsci.2014.04.003
8. Kaneko K, Yadav N, Takeuchi K, Maira B, Terano M, Taniike T (2014) Versatile strategy for fabrication of polypropylene nano-composites with inorganic network structures based on catalyzed in-situ sol–gel reaction during melt mixing. Compos Sci Technol 102:120–125. https://doi.org/10.1016/j.compscitech.2014.07.024
9. Bahloul W, Bounor-Legaré V, Seytre G, Cassagnau P (2011) Influence of a non-polar medium (alkane and molten polypropylene) on the titanium n-butoxide hydrolysis-condensation reactions. J Sol-Gel Sci Technol 57:86–94. https://doi.org/10.1007/s10971-010-2327-1
10. Bahloul W (2010) Génération in situ de dioxyde de titane par réactions d'hydrolyse-condensations dans une matrice polymère fondu. Thesis, Lyon 1. http://www.theses.fr/2010LYO10124. Accessed 25 Jun 2019
11. Niederberger M, Pinna N (2009) Aqueous and nonaqueous sol-gel chemistry. In: Metal oxide nanoparticles in organic solvents. Springer, London, p 7–18. http://link.springer.com/10.1007/978-1-84882-671-7_2. Accessed 24 Jan 2017

12. Mutin PH, Vioux A (2013) Recent advances in the synthesis of inorganic materials via non-hydrolytic condensation and related low-temperature routes. J Mater Chem A 1:11504. https://doi.org/10.1039/c3ta12058a

13. Vioux A (1997) Nonhydrolytic sol−gel routes to oxides. Chem Mater 9:2292–2299. https://doi.org/10.1021/cm970322a

14. Niederberger M, Garnweitner G (2006) Organic reaction pathways in the nonaqueous synthesis of metal oxide nanoparticles. Chem Eur J 12:7282–7302. https://doi.org/10.1002/chem.200600313

15. Trentler TJ, Denler TE, Bertone JF, Agrawal A, Colvin VL (1999) Synthesis of TiO2 nanocrystals by nonhydrolytic solution-based reactions. J Am Chem Soc 121:1613–1614. https://doi.org/10.1021/ja983361b

16. Niederberger M, Bard MH, Stucky GD (2002) Benzyl alcohol and transition metal chlorides as a versatile reaction system for the nonaqueous and low-temperature synthesis of crystalline nano-objects with controlled dimensionality. J Am Chem Soc 124:13642–13643. https://doi.org/10.1021/ja027115i

17. Wang Y, Kim S, Louvain N, Alauzun JG, Mutin PH (2019) Acetic anhydride as an oxygen donor in the non-hydrolytic sol–gel synthesis of mesoporous TiO2 with high electrochemical lithium storage performances. Chem – A Eur J 25:4767–4774. https://doi.org/10.1002/chem.201806073

18. Morselli D, Messori M, Bondioli F (2011) Poly(methyl methacrylate)-TiO2 nanocomposite obtained by non-hydrolytic sol–gel synthesis. J Mater Sci 46:6609–6617. https://doi.org/10.1007/s10853-011-5610-9

19. Scarpelli F, Godbert N (2018) Mesoporous TiO2 thin films: state of the art. https://doi.org/10.5772/intechopen.74244

20. Mofokeng JP, Luyt AS, Tábi T, Kovács J (2012) Comparison of injection moulded, natural fibre-reinforced composites with PP and PLA as matrices. J Thermoplast Composite Mater 25:927–948. https://doi.org/10.1177/0892705711423291

21. Longo C, Savaris M, Zeni M, Brandalise RN, Grisa AMC (2011) Degradation study of polypropylene (PP) and bioriented polypropylene (BOPP) in the environment. Mater Res 14:442–448. https://doi.org/10.1590/S1516-14392011005000080

22. Day M, Cooney JD, MacKinnon M (1995) Degradation of contaminated plastics: a kinetic study. Polym Degrad Stab 48:341–349. https://doi.org/10.1016/0141-3910(95)00088-4

23. Esthappan S, Kumbamala Kuttappan S, Joseph R (2012) Thermal and mechanical properties of polypropylene/titanium dioxide nanocomposite fibers. Mater Des 37:537–542. https://doi.org/10.1016/j.matdes.2012.01.038

24. Aydemir D, Uzun G, Gumus H, Yıldız S, Gumus S, BARDAK T, Gündüz G (2016) Nanocomposites of polypropylene/nano titanium dioxide: effect of loading rates of Nano–TiO2. Mater Sci 22:364–369. https://doi.org/10.5755/j01.ms.22.3.8217

25. Lannon JM, Meng Q (1999) Analysis of a poly(propylene)(PP) homopolymer by XPS. Surf Sci Spectra 6:79–82. https://doi.org/10.1116/1.1247902

26. Bahloul W, Mélis F, Bounor-Legaré V, Cassagnau P (2012) Structural characterization and antibacterial activity of PP/TiO2 nanocomposites prepared by an in situ sol–gel method. Mater Chem Phys 134:399–406. https://doi.org/10.1016/j.matchemphys.2012.03.008

27. Hamden Z, Bouattour S, Ferraria AM, Ferreira DP, Vieira Ferreira LF, Botelho do Rego AM, Boufi S (2016) In situ generation of TiO2 nanoparticles using chitosan as a template and their photocatalytic activity. J Photochemistry Photobiol A: Chem 321:211–222. https://doi.org/10.1016/j.jphotochem.2016.02.008

28. Barlier V, Bounor-Legaré V, Boiteux G, Davenas J, Léonard D (2008) Hydrolysis–condensation reactions of titanium alkoxides in thin films: a study of the steric hindrance effect by X-ray photoelectron spectroscopy. Appl Surf Sci 254:5408–5412. https://doi.org/10.1016/j.apsusc.2008.02.076

29. Ge L, Xu M, Fang H, Sun M (2006) Preparation of TiO2 thin films from autoclaved sol containing needle-like anatase crystals. Appl Surf Sci 253:720–725. https://doi.org/10.1016/j.apsusc.2005.12.162

30. Gao Y, Masuda Y, Koumoto K (2004) Light-excited super-hydrophilicity of amorphous TiO2 thin films deposited in an aqueous peroxotitanate solution. Langmuir 20:3188–3194. https://doi.org/10.1021/la0303207

31. Shaikh T, Rathore A, Kaur H (2017) Poly (Lactic Acid) grafting of TiO2 nanoparticles: a shift in dye Degradation performance of TiO2 from UV to solar light. ChemistrySelect 2:6901–6908. https://doi.org/10.1002/slct.201701560

32. Huang PJ, Chang H, Yeh CT, Tsai CW (1997) Phase transformation of TiO2 monitored by Thermo-Raman spectroscopy with TGA/DTA. Thermochim Acta 297:85–92. https://doi.org/10.1016/S0040-6031(97)00168-8

33. Karacan I, Benli H (2011) An X-ray diffraction study for isotactic polypropylene fibers produced with take-up speeds of 2500-4250 m/min. Tekst ve Konfeksiyon 21:201–209

34. Sakurai K, Mizusawa M (2010) X-ray diffraction imaging of anatase and rutile. Anal Chem 82:3519–3522. https://doi.org/10.1021/ac9024126

35. Hu Q, Marand E (1999) In situ formation of nanosized TiO2 domains within poly(amide–imide) by a sol–gel process. Polymer 40:4833–4843. https://doi.org/10.1016/S0032-3861(98)00264-X

36. Wu C-S (2004) In situ polymerization of titanium isopropoxide in polycaprolactone: properties and characterization of the hybrid nanocomposites. J Appl Polym Sci 92:1749–1757. https://doi.org/10.1002/app.20135

37. Fedors RF (1974) A method for estimating both the solubility parameters and molar volumes of liquids. Polym Eng Sci 14:147–154. https://doi.org/10.1002/pen.760140211

38. Michaels AS, Vieth WR, Alcalay HH (1968) The solubility parameter of polypropylene. J Appl Polym Sci 12:1621–1624. https://doi.org/10.1002/app.1968.070120711

39. Onuoha C, Onyemaobi O, Anyakwo C, Onuegbu G (2017) Morphology and physical/end-use properties of recycled polypropylene-corn cob powder composites. Int J Eng Technol 11:1–12. https://doi.org/10.18052/www.scipress.com/IJET.11.1

40. Bahloul W, Bounor-Legaré V, David L, Cassagnau P (2010) Morphology and viscoelasticity of PP/TiO2 nanocomposites prepared by in situ sol–gel method. J Polym Sci Part B: Polym Phys 48:1213–1222. https://doi.org/10.1002/polb.22012

41. Cassagnau P (2008) Melt rheology of organoclay and fumed silica nanocomposites. Polymer 49:2183–2196. https://doi.org/10.1016/j.polymer.2007.12.035

42. Zhang Q, Archer LA (2002) Poly(ethylene oxide)/silica nanocomposites: structure and rheology. Langmuir 18:10435–10442. https://doi.org/10.1021/la026338j

43. Acierno D, Filippone G, Romeo G, Russo P (2007) Rheological aspects of PP-TiO2 micro and nanocomposites: a preliminary investigation. Macromol Symp 247:59–66. https://doi.org/10.1002/masy.200750108

44. Lacoste J-F, Bounor-Legaré V, Llauro M-F, Monnet C, Cassagnau P, Michel A (2005) Functionalization of poly(ethylene terephthalate) in the melt state: chemical and rheological aspects. J Polym Sci Part A: Polym Chem 43:2207–2223. https://doi.org/10.1002/pola.20696

45. Haroponiatowski E, Rodrigueztalavera R, Delacruzheredia M, Canocorona O, Arroyomurillo R (1994) Crystallization of nano-sized titania particles prepared by the sol-gel process. J Mater Res 9:2102–2108. https://doi.org/10.1557/JMR.1994.2102

46. Parker J, Siegel R (1990) Raman microprobe study of nanophase TiO2 and oxidation-induced spectral changes. J Mater Res 5:1246–1252. https://doi.org/10.1557/JMR.1990.1246